




Emergent quadrupolar order in the spin- $\frac{1}{2}$ Kitaev-Heisenberg model

Manodip Routh ^{1,*} Sayan Ghosh,^{1,*} Jeroen van den Brink,^{2,3,4} Satoshi Nishimoto ^{2,4,†} and Manoranjan Kumar ^{1,‡}

¹*S. N. Bose National Centre for Basic Sciences, Kolkata 700098, India*

²*Institute for Theoretical Solid State Physics, IFW Dresden, 01069 Dresden, Germany*

³*Würzburg-Dresden Cluster of Excellence ct.qmat, 97074 Würzburg, Germany*

⁴*Department of Physics, Technical University Dresden, 01069 Dresden, Germany*



(Received 9 January 2024; revised 4 May 2024; accepted 20 May 2024; published 5 June 2024)

Motivated by the largely unexplored domain of multipolar ordered spin states in the Kitaev-Heisenberg (KH) systems we investigate the ground state dynamics of the spin- $\frac{1}{2}$ KH model, focusing on quadrupolar (QP) order in two-leg ladder and two-dimensional honeycomb lattice geometries. Employing exact diagonalization and density-matrix renormalization group methods, we analyze the QP order parameter and correlation functions. Our findings reveal a robust QP order across a wide range of the phase diagram, influenced by the interplay between Heisenberg and Kitaev interactions. Notably, we observe an enhancement of QP order near Kitaev quantum spin-liquid (QSL) phases, despite the absence of long-range spin-spin correlations. This highlights a complex relationship between QP order and QSLs, offering different insights into quantum magnetism in low-dimensional systems. Our findings provide a rational explanation for the observed nonlinear magnetic susceptibility in α -RuCl₃.

DOI: [10.1103/PhysRevB.109.L220403](https://doi.org/10.1103/PhysRevB.109.L220403)

Introduction. Quantum spin liquids (QSLs) represent a quantum phase of matter that challenges traditional understanding by lacking magnetic long-range order (LRO), yet they may exhibit global topological order [1]. These elusive states emerge in frustrated magnetic systems, where competing spin-exchange interactions not only foster the QSL state but also lead to complex entangled states such as dimer formations, fractional excitations such as spinons, and Majorana excitations in the ground state (gs) [2–10]. A key development in understanding QSLs was the Kitaev model, which proposed spin- $\frac{1}{2}$ particles on a hexagonal lattice with direction-dependent exchange interactions, introducing frustration into the system [11]. The gs of this model is a QSL, characterized by Majorana fermions and gauge vortices as elementary excitations [12–17].

The experimental pursuit of the Kitaev model has prominently featured iridium-based materials such as A₂IrO₃ (A = Na, Li), where Ir atoms form a honeycomb structure [18,19]. In these materials, the octahedral coordination of ligands induces a crystal field, splitting the Ir *d* orbitals into *t*_{2g} and *e*_g levels. Strong spin-orbit coupling further splits the *t*_{2g} orbitals, allowing the two highest states of each to mimic effective spin- $\frac{1}{2}$ degrees of freedom. This results in orbital-dependent, directionally anisotropic spin exchanges, i.e., so-called Kitaev interactions [20]. However, the Kitaev-Heisenberg (KH) model, incorporating residual nearest-neighbor Heisenberg interactions, offers a more realistic description of the magnetic properties of these materials [21]. Similar Hamiltonians have

been proposed for materials such as α -RuCl₃ [20,22–26], β -Li₂IrO₃ [20,25–28], and γ -Li₂IrO₃ [20,29].

The gs phase diagram of the KH model on honeycomb-lattice KH model has been extensively studied, revealing four magnetic LRO phases [Néel, zigzag (ZZ), stripy (ST), and ferromagnetic (FM)] and two QSL phases [FM Kitaev (FK) and antiferromagnetic Kitaev (AFK) QSLs], by tuning the Heisenberg and Kitaev interactions [21,30–32]. However, the potential for a quantum phase involving multipolar spin states, such as a quadrupolar (QP) or spin-nematic state, in the KH model remains largely unexplored. From an experimental perspective, third-order positive susceptibility probing a higher-order correlation such as QP has been observed at zero magnetic field in α -RuCl₃ [33]. Yet, the intricate mechanisms behind these observations are not fully elucidated. In addition to these experimental findings, the present Letter is further motivated by the inclusion of a staggered QP operator in the Hamiltonian of the KH model (see below).

The QP phase, established in liquid-crystal systems [34–37], manifests in magnetic systems as spin nematics, where magnetic quadrupole moments create orientational order without magnetic LRO [38–40]. Initially identified in spin-1 systems with biquadratic exchange [41], this order has been explored in various Heisenberg spin-1 models [42–44]. Extending this concept to spin- $\frac{1}{2}$ systems has spurred research, particularly in *J*₁-*J*₂ chain systems under strong magnetic fields [45–47]. In the context of Kitaev systems, a spin-nematic phase in the spin- $\frac{1}{2}$ Kitaev-Ising model has been predicted, arising from the interplay between Kitaev QSL and magnetic LRO, but lacking topological order [48]. Additionally, four-body interactions among Majorana fermions in the Kitaev QSL could induce a topological nematic phase transition, evolving from the chiral QSL phase to the toric code phase [49].

*These authors contributed equally to this work.

†s.nishimoto@ifw-dresden.de

‡manoranjan.kumar@bose.res.in

In this Letter, we explore the gs dynamics of the spin- $\frac{1}{2}$ KH model, focusing on the QP order. We investigate two geometries, the two-leg ladder and the two-dimensional (2D) honeycomb lattice, using exact diagonalization (ED) and density-matrix renormalization group (DMRG) methods. Our primary contribution is a detailed exploration of the QP order parameter and correlation functions within these systems. We present a different gs phase diagram highlighting the QP order as a function of the ratio between Heisenberg and Kitaev interactions. A striking aspect of our findings is the robust presence and stability of QP order across a wide range of the phase diagram, with a notable enhancement near the Kitaev QSL phases. This enhancement occurs despite the absence of longer-range spin-spin correlations, adding another dimension to our understanding of the interplay between QP order and QSLs.

Quadrupolar operator. The QP state emerges as a quantum ordered phase characterized by collective bimagnon excitations. This intriguing state, while exhibiting a preference for the orientation of paired magnons, notably does not break time-reversal symmetry. Its detection hinges on the analysis of a symmetric and traceless rank-2 tensor operator [50],

$$\hat{Q}_{kl}^{\alpha\beta} = S_k^\alpha S_l^\beta + S_l^\alpha S_k^\beta - \frac{2}{3}(S_k \cdot S_l)\delta_{\alpha\beta}, \quad (1)$$

where α and β represent the Cartesian coordinates such as x, y, z and k, l denote different sites.

Model. We consider a spin- $\frac{1}{2}$ KH model on both a ladder and a honeycomb lattice [21]. The Hamiltonian is given by

$$\mathcal{H} = J \sum_{k,l} \vec{S}_k \cdot \vec{S}_l + K \sum_{\gamma} \sum_{k,l} S_k^\gamma S_l^\gamma, \quad (2)$$

where S_k^γ is the γ ($=x, y, \text{ or } z$) component of the spin- $\frac{1}{2}$ operator \vec{S}_k at site k . Here, J and K denote the Heisenberg and Kitaev interactions, respectively. To facilitate analysis, we introduce an angular parameter ϕ ($\in [0, 2\pi]$), defining $J = \cos \phi$ and $K = \sin \phi$.

For the ladder or cylinder geometry, the Hamiltonian is adapted to include the spin- $\frac{1}{2}$ operator $\vec{S}_{i,j}$ at site i on the j th leg:

$$\begin{aligned} \mathcal{H}_{\text{leg}} &= \frac{2J+K}{4} \sum_{j=1}^n \sum_{i=1}^L (S_{i,j}^+ S_{i+1,j}^- + S_{i,j}^- S_{i+1,j}^+) \\ &+ \frac{K}{2} \sum_{j=1}^n \sum_{i=1}^L (-1)^{i+j} (\hat{Q}_{ij}^{x^2-y^2}) + J \sum_{j=1}^n \sum_{i=1}^L (S_{i,j}^z S_{i+1,j}^z) \\ &\equiv \mathcal{H}_{\text{exc}} + \mathcal{H}_Q + \mathcal{H}_z. \end{aligned} \quad (3)$$

In this formulation, \mathcal{H}_Q explicitly includes a specific component of Eq. (1), which signifies the QP operator,

$$\hat{Q}_{ij}^{x^2-y^2} = \frac{1}{2}(S_{i,j}^+ S_{i+1,j}^+ + S_{i,j}^- S_{i+1,j}^-). \quad (4)$$

Its dominance suggests the potential stabilization of QP order. The possibility of QP order arising through similar mechanisms has been previously discussed in the context of J_1 - J_2 chain systems under magnetic fields [51].

Although the Kitaev model was originally proposed for the honeycomb lattice, it is recognized that any three-coordinated lattice with Kitaev interactions can exhibit similar intriguing

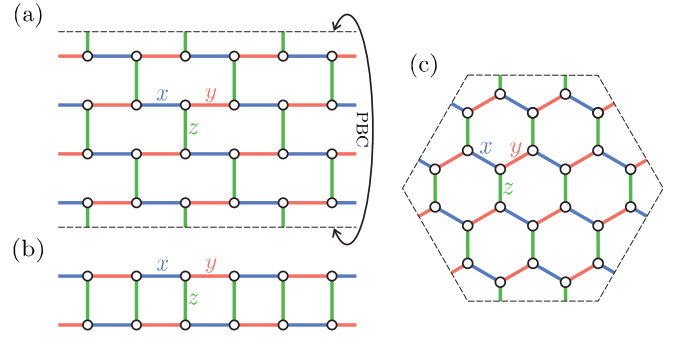


FIG. 1. Lattice structures used in our calculations: (a) KH ladder or brickwall lattice which is obtained by deforming the honeycomb lattice KH model. (b) Two-leg KH ladder. (c) A 24-site honeycomb lattice KH cluster with periodic boundary conditions.

properties. In this sense, the KH model on a two-leg ladder [Fig. 1(b)], derived from a brickwall lattice analogous to the honeycomb lattice, aligns with the necessary geometry. This alignment indicates that the two-leg KH ladder can offer vital insights into the behavior of the 2D honeycomb lattice KH model. Notably, the gs phase diagram of the ladder model displays significant similarities with the 2D counterpart in terms of magnetic order and Kitaev QSL, with the key distinction being the replacement of the Néel phase by the rung-singlet (RS) phase [52,53]. Therefore, initiating our investigation with the two-leg KH ladder is a strategic choice. This setup not only allows for precise numerical calculations but also facilitates reliable extrapolations to the thermodynamic limit, essential for exploring novel phenomena in the 2D KH model. Building upon this, we extend our investigation to four-leg and six-leg cylinders [Fig. 1(a)], progressively approaching the 2D bulk limit. This systematic increase in the number of legs serves to bridge our understanding from the simpler ladder systems to the more complex dynamics inherent in the full 2D KH model.

Methods. To investigate the intricate dynamics of the KH model, we employ two complementary computational techniques. For the two-leg ladder system [Fig. 1(b)], encompassing system sizes up to 12×2 , and for the 24-site periodic boundary condition (PBC) cluster [Fig. 1(c)], we utilize the exact diagonalization (ED) method. For larger systems, specifically extended two-leg ladders, as well as four-leg and six-leg cylinders [Fig. 1(a)], we implement the DMRG method [54–56]. In our DMRG calculations, we retain up to 5000 density-matrix eigenstates during the renormalization process. This high number of kept states ensures the accuracy of our results, with the largest discarded weight being maintained at approximately 2×10^{-5} .

Quadrupolar order in the two-leg ladder. We commence our analysis with the two-leg ladder system. To obtain a comprehensive phase diagram for QP order as a function of ϕ , we calculate the QP order parameter $\langle \hat{Q}_{ij}^{x^2-y^2} \rangle$ using ED. Our findings, focusing on a single bond along the leg, are depicted in Fig. 2(a). We find that $\langle \hat{Q}_{ij}^{x^2-y^2} \rangle$ exhibits finite values over a broad range of ϕ ($0.48\pi \lesssim \phi \lesssim 1.56\pi$) with minimal finite-size effects. This order parameter

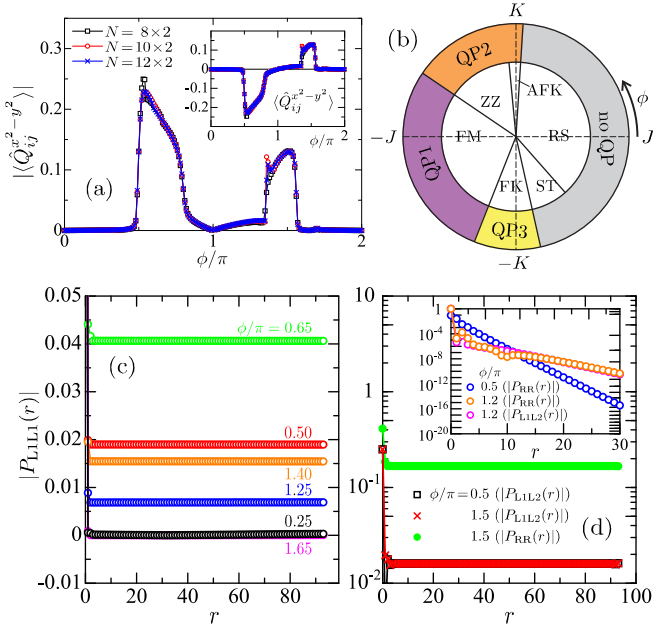


FIG. 2. Results for two-leg KH ladder. (a) Absolute values of the QP order parameter for leg bonds with various system sizes. The inset represents the same physical quantity but without taking absolute values. (b) Ground state phase diagram for magnetic order (inner) and QP order (outer). Four long-range ordered phases: rung-singlet (RS), zigzag (ZZ), ferromagnetic (FM), stripy (ST); and two QSL phases: antiferromagnetic Kitaev (AFK) and ferromagnetic Kitaev (FK). (c) Compilation of the behavior of the QP correlation functions $|P_{LIL1}(r)|$ with $N = 100 \times 2$ cluster for representative parameters (see text). (d) Interleg and rung-rung QP correlation functions at $\phi/\pi = 0.5, 1.2,$ and 1.5 . Inset: Examples for the cases where the QP correlation function exhibits an exponential decay.

shows significant values in the AFK, FK, and ZZ phases of the magnetic phase diagram, while it rather diminishes in the FM phase [Fig. 2(b)]. Conversely, when i and j are positioned on a rung bond, $\langle \hat{Q}_{ij}^{x^2-y^2} \rangle$ consistently equals zero.

To further substantiate these findings, using DMRG we compute leg-leg and rung-rung QP correlation functions, defined as

$$P_{LmLn}(r) = \langle S_{i,m}^+ S_{i+1,m}^+ S_{i+r,n}^- S_{i+1+r,n}^- \rangle \quad (5)$$

and

$$P_{RR}(r) = \langle S_{i,m}^+ S_{i,m+1}^+ S_{i+r,m}^- S_{i+r,m+1}^- \rangle, \quad (6)$$

respectively. The results, summarized in Figs. 2(c) and 2(d), reveal that the intraleg correlation $P_{LIL1}(r)$ exhibits QP LRO within the ϕ range where $\langle \hat{Q}_{ij}^{x^2-y^2} \rangle$ is finite. Note that $P_{LIL1}(r)$ alternates in sign with distance. Meanwhile, near both Kitaev points $\phi = \pm\pi/2$, the interleg correlation $P_{LIL2}(r)$, and near the FK phase, the rung-rung correlation $P_{RR}(r)$, also exhibit QP LRO. Unlike $P_{LIL1}(r)$, both $P_{LIL2}(r)$ and $P_{RR}(r)$ are always positive. Interestingly, despite the rung QP order parameter being consistently zero across all ϕ values, $P_{RR}(r)$ still exhibits LRO in the FK phase. This suggests that states of QP order with broken spin-rotational symmetry are

degenerate, leading to a zero local order parameter, yet detectable through correlation functions.

From these correlation function analyses, the ϕ domain for QP order can be classified into four phases: QP1 [only $P_{LIL1}(r)$ shows LRO], QP2 [both $P_{LIL1}(r)$ and $P_{LIL2}(r)$ show LRO], QP3 [all of $P_{LIL1}(r)$, $P_{LIL2}(r)$, and $P_{RR}(r)$ show LRO], and a phase with no QP LRO. The schematic picture of each QP phase is illustrated in the Supplemental Material [57]. The correspondence with the magnetic order phases is shown in the phase diagram in Fig. 2(b). The phase diagram for QP order can be correlated by considering the spin structures of the corresponding magnetic phases and we notice that in the presence of a dominant QP phase along the x^2-y^2 plane the magnetic order either vanishes or appears along the z axis. In the FM phase ($0.81 \lesssim \phi/\pi \lesssim 1.38$), the near-full magnetization results in smaller values of $P_{LIL1}(r)$ and $|\langle \hat{Q}_{ij}^{x^2-y^2} \rangle|$, and they vanish without \mathcal{H}_Q at $\phi = \pi$. The ZZ phase ($0.53 \lesssim \phi/\pi \lesssim 0.81$) exhibits Ising-type LRO in each leg with opposite polarization between legs [52], leading to the anticipated development of $P_{LIL2}(r)$. However, $P_{RR}(r)$ does not show LRO due to antiparallel spin orientation on the rungs. In fact, a detailed wave-function analysis suggests the dominant contribution of double-flip configurations in the gs (see the Supplemental Material [57]). In the RS ($-0.26 \lesssim \phi/\pi \lesssim 0.48$) and ST ($1.57 \lesssim \phi/\pi \lesssim 1.74$) phases, the each leg possesses a Néel-type LRO, precluding the dominance of the \mathcal{H}_Q term. Thus, a QP order is absent.

In the AFK ($0.48 \lesssim \phi/\pi \lesssim 0.53$) and FK ($1.38 \lesssim \phi/\pi \lesssim 1.57$) phases, the competition between dipole fluctuations (\mathcal{H}_{exc}) and QP fluctuations (\mathcal{H}_Q) complicates gs determination. Nevertheless, the larger coefficient of \mathcal{H}_Q supports the emergence of QP order along the leg, as corroborated by our numerical results. Remarkably, in the FK phase, the rung QP correlation function $P_{RR}(r)$ also exhibits LRO, with a saturation value exceeding $P_{LIL1}(r)$. This is attributed to the FM Ising character of rung interactions, conducive to bimagnon formation [58]. The approximate wave function of the FK phase is detailed in the Supplemental Material [57].

Given these insights, we hypothesize that QP order might also be present in the 2D honeycomb KH system, akin to the two-leg ladder scenario. To test this hypothesis, we extend our investigation to isotropic honeycomb cluster as well as four-leg and six-leg cylinders, in the parts that follow.

Quadrupolar order in the 2D honeycomb lattice. Analogous to the approach for the two-leg ladder, we first aim to grasp the overall picture of the QP order phase diagram as a function of ϕ by calculating the QP order parameter using ED on the 24-site PBC cluster. The results, illustrated in Fig. 3(a), are compared with those from the two-leg ladder. In the context of magnetic order phases for the 2D honeycomb lattice KH model, the QP order parameter is finite in the AFK ($0.494 \lesssim \phi/\pi \lesssim 0.506$), ZZ ($0.506 \lesssim \phi/\pi \lesssim 0.847$), FM ($0.847 \lesssim \phi/\pi \lesssim 1.452$), FK ($1.452 \lesssim \phi/\pi \lesssim 1.539$), and ST ($1.539 \lesssim \phi/\pi \lesssim 1.694$) phases, and it is zero only in the Néel phase ($-0.306 \lesssim \phi/\pi \lesssim 0.494$). While the results are fundamentally similar to those for the two-leg ladder, a notable difference is that the QP order parameter remains finite even in the ST phase. For the z bonds, similar

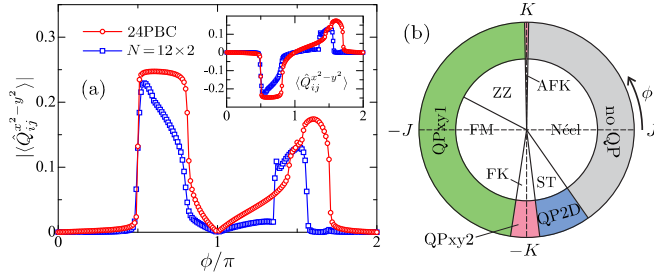


FIG. 3. Results for honeycomb lattice KH model. (a) Absolute values of the QP order parameter for the x or y bond, calculated using the 24-site PBC cluster. For comparison, those for the two-leg KH ladder are also plotted. The inset represents the same physical quantity but without taking absolute values. (b) Ground state phase diagram for magnetic order (inner) and QP order (outer).

to the rung QP in the two-leg ladder, the QP order parameter is zero.

To ascertain the persistence of QP order in the bulk limit, we compute QP correlation functions using DMRG for four-leg and six-leg cylinders, in addition to the two-leg ladder. Focusing on the intraleg QP correlation function, $P_{L1L1}(r)$, we observe in Fig. 4 that, consistent with the QP order parameter results, $P_{L1L1}(r)$ converges to a finite value in the long-distance limit for all magnetic phases except the Néel phase. Importantly, this convergence value does not diminish with an increasing number of legs, suggesting its stability in the bulk limit. In the Néel phase, $P_{L1L1}(r)$ exhibits a power-law decay indicating no long-range QP order.

The decay of QP correlation functions perpendicular to the leg direction, namely along the z bond, is also of interest. We calculate the interleg QP correlation function, $P_{L1Ln}(r)$, for various leg distances in a 50×6 system. The calculated

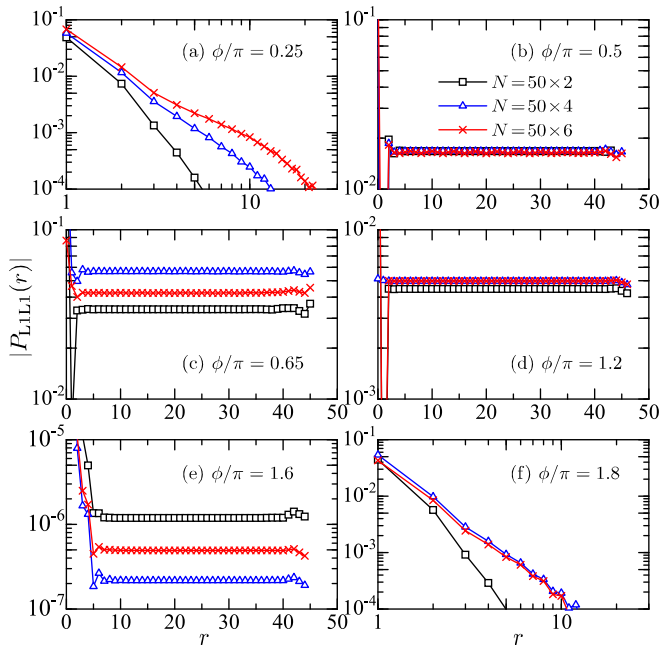


FIG. 4. DMRG results for the QP correlation functions $P_{L1L1}(r)$ at representative value of ϕ for six quantum phases using two-leg, four-leg, and six-leg cylinders.

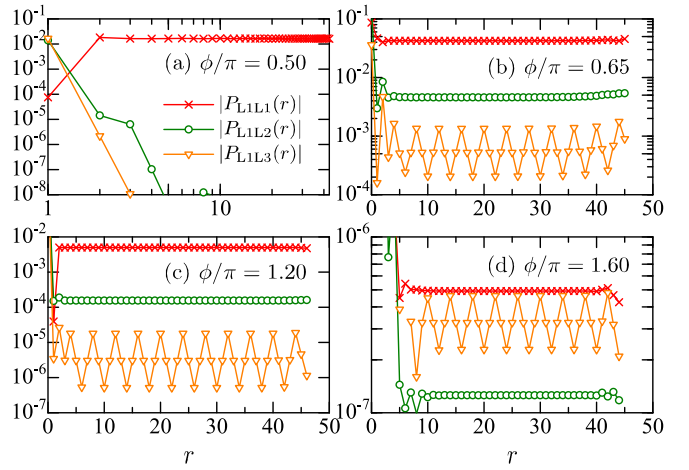


FIG. 5. DMRG results for the interleg QP correlation functions, $P_{L1Ln}(r)$ for $n=1-3$ at magnetic ordered phases, including ZZ ($\phi/\pi = 0.65$), FM ($\phi/\pi = 1.2$), ST ($\phi/\pi = 1.6$), and QSL phase ($\phi/\pi = 0.5$), using six-leg cylinders.

$P_{L1Ln}(r)$ for $n=1-3$ is plotted in Fig. 5. In the ZZ and FM phases, the saturation value of $P_{L1Ln}(r)$ at long distances follows power-law decay [Figs. 5(b) and 5(c)], suggesting quasi-LRO along the z -bond direction (QPxy1 phase). Near the Kitaev points (AFK and FK), a rapid decay of interleg correlations is observed [Fig. 5(a)], indicating LRO in the xy zigzag direction alone (QPxy2 phase). The ST phase presents a unique case, where the decay along the z -bond direction does not follow a simple pattern [Fig. 5(d)], hinting at the potential for LRO (QP2D phase). For all ϕ values, the rung-rung QP correlation function, $P_{RR}(r)$, exhibits exponential decay for both four-leg and six-leg cylinders. The QP phases are explained in detail in the Supplemental Material [57]. The correspondence between QP order and magnetic order is summarized in the phase diagram in Fig. 3(b). A notable distinction from the two-leg ladder case is the presence of QP order in the ST phase, likely due to the unique orientation of ST order in this setting, although the magnitude of QP correlations in this phase is relatively small compared to other phases.

Summary. We have explored the gs dynamics of the spin- $\frac{1}{2}$ KH model, focusing particularly on the emergence and characteristics of QP order. Our study spans two distinct geometries: the two-leg ladder and the 2D honeycomb lattice. Employing a synergistic approach combining ED and DMRG techniques, we have meticulously analyzed the QP order parameter and correlation functions in these systems. Our key contribution is the unveiling of a comprehensive gs phase diagram, which distinctly maps out the QP order in relation to the interplay between Heisenberg and Kitaev interactions. A notable discovery is the pronounced stability of QP order across a broad range of the phase diagram, underscoring its robustness in the KH model. Additionally, our findings reveal a remarkable enhancement of the QP order parameter and its correlation functions near the Kitaev QSL phases. This enhancement is particularly intriguing as it occurs in the absence of long-range spin-spin correlations, suggesting a nuanced relationship between QP order and QSLs. In fact, the

third-order positive susceptibility, indicative of a general signature of QP order, has been observed in α -RuCl₃ [33], where the relationship between K and J appears to be $-K \gg J > 0$ [59], suggesting a proximity to the FK QSL phase.

These insights not only advance our understanding of the KH model but also contribute significantly to the broader discourse on quantum magnetism in low-dimensional systems, highlighting the intricate interplay between different types of quantum order.

Acknowledgments. M.K. thanks Saptarshi Mandal, Krishnendu Sengupta, David Logan, Jay D. Sau, and Rajiv R. P.

Singh for the fruitful discussions. We thank Ulrike Nitzsche for technical assistance. M.K. acknowledges support from SERB through Grant Sanction No. CRG/2020/000754. M.R. acknowledges the financial support from Institute for Theoretical Solid State Physics of IFW Dresden and DST-India. S.G. expresses appreciation for financial support from DST-INSPIRE. This project is funded by the German Research Foundation (DFG) via the projects A05 of the Collaborative Research Center SFB 1143 (Project-id 247310070) and through the Wurzburg-Dresden Cluster of Excellence on Complexity and Topology in Quantum Matter ct.qmat (EXC 2147, Project No. 39085490).

-
- [1] L. Balents, Spin liquids in frustrated magnets, *Nature (London)* **464**, 199 (2010).
- [2] C. Broholm, R. J. Cava, S. A. Kivelson, D. G. Nocera, M. R. Norman, and T. Senthil, Quantum spin liquids, *Science* **367**, eaay0668 (2020).
- [3] Y. Zhou, K. Kanoda, and T.-K. Ng, Quantum spin liquid states, *Rev. Mod. Phys.* **89**, 025003 (2017).
- [4] L. Savary and L. Balents, Quantum spin liquids: A review, *Rep. Prog. Phys.* **80**, 016502 (2017).
- [5] M. Enderle, B. Fåk, H.-J. Mikeska, R. K. Kremer, A. Prokofiev, and W. Assmus, Two-spinon and four-spinon continuum in a frustrated ferromagnetic spin-1/2 chain, *Phys. Rev. Lett.* **104**, 237207 (2010).
- [6] J. Schlappa, U. Kumar, K. Zhou, S. Singh, M. Mourigal, V. Strocov, A. Revcolevschi, L. Patthey, H. Rønnow, S. Johnston *et al.*, Probing multi-spinon excitations outside of the two-spinon continuum in the antiferromagnetic spin chain cuprate Sr₂CuO₃, *Nat. Commun.* **9**, 5394 (2018).
- [7] S.-H. Do, S.-Y. Park, J. Yoshitake, J. Nasu, Y. Motome, Y. S. Kwon, D. Adroja, D. Voneshen, K. Kim, T.-H. Jang *et al.*, Incarnation of Majorana fermions in Kitaev quantum spin lattice, [arXiv:1703.01081](https://arxiv.org/abs/1703.01081).
- [8] A. Koga, Y. Murakami, and J. Nasu, Majorana correlations in the Kitaev model with ordered-flux structures, *Phys. Rev. B* **103**, 214421 (2021).
- [9] D. Wulferding, Y. Choi, S.-H. Do, C. H. Lee, P. Lemmens, C. Faugeras, Y. Gallais, and K.-Y. Choi, Magnon bound states versus anyonic Majorana excitations in the Kitaev honeycomb magnet α -RuCl₃, *Nat. Commun.* **11**, 1603 (2020).
- [10] A. Hashimoto, Y. Murakami, and A. Koga, Majorana excitations in the anisotropic Kitaev model with an ordered-flux structure, *J. Phys.: Conf. Ser.* **2164**, 012028 (2022).
- [11] A. Kitaev, Anyons in an exactly solved model and beyond, *Ann. Phys.* **321**, 2 (2006).
- [12] M. Hermanns, K. O'Brien, and S. Trebst, Weyl spin liquids, *Phys. Rev. Lett.* **114**, 157202 (2015).
- [13] K. Le Hur, A. Soret, and F. Yang, Majorana spin liquids, topology, and superconductivity in ladders, *Phys. Rev. B* **96**, 205109 (2017).
- [14] S. Mandal, S. Bhattacharjee, K. Sengupta, R. Shankar, and G. Baskaran, Confinement-deconfinement transition and spin correlations in a generalized Kitaev model, *Phys. Rev. B* **84**, 155121 (2011).
- [15] G. Baskaran, S. Mandal, and R. Shankar, Exact results for spin dynamics and fractionalization in the Kitaev model, *Phys. Rev. Lett.* **98**, 247201 (2007).
- [16] G. Baskaran, D. Sen, and R. Shankar, Spin-S Kitaev model: Classical ground states, order from disorder, and exact correlation functions, *Phys. Rev. B* **78**, 115116 (2008).
- [17] G. Baskaran, Metastable Kitaev spin liquids in isotropic quantum Heisenberg magnets, [arXiv:2309.07119](https://arxiv.org/abs/2309.07119).
- [18] Y. Singh, S. Manni, J. Reuther, T. Berlijn, R. Thomale, W. Ku, S. Trebst, and P. Gegenwart, Relevance of the Heisenberg-Kitaev model for the honeycomb lattice iridates A₂IrO₃, *Phys. Rev. Lett.* **108**, 127203 (2012).
- [19] S. Hwan Chun, J.-W. Kim, J. Kim, H. Zheng, C. C. Stoumpos, C. Malliakas, J. Mitchell, K. Mehlawat, Y. Singh, Y. Choi *et al.*, Direct evidence for dominant bond-directional interactions in a honeycomb lattice iridate Na₂IrO₃, *Nat. Phys.* **11**, 462 (2015).
- [20] S. Trebst and C. Hickey, Kitaev materials, *Phys. Rep.* **950**, 1 (2022).
- [21] J. Chaloupka, G. Jackeli, and G. Khaliullin, Kitaev-Heisenberg model on a honeycomb lattice: Possible exotic phases in iridium oxides A₂IrO₃, *Phys. Rev. Lett.* **105**, 027204 (2010).
- [22] H. Suzuki, H. Liu, J. Bertinshaw, K. Ueda, H. Kim, S. Laha, D. Weber, Z. Yang, L. Wang, H. Takahashi *et al.*, Proximate ferromagnetic state in the Kitaev model material α -RuCl₃, *Nat. Commun.* **12**, 4512 (2021).
- [23] S.-H. Do, S.-Y. Park, J. Yoshitake, J. Nasu, Y. Motome, Y. S. Kwon, D. Adroja, D. Voneshen, K. Kim, T.-H. Jang *et al.*, Majorana fermions in the Kitaev quantum spin system α -RuCl₃, *Nat. Phys.* **13**, 1079 (2017).
- [24] A. Banerjee, J. Yan, J. Knolle, C. A. Bridges, M. B. Stone, M. D. Lumsden, D. G. Mandrus, D. A. Tennant, R. Moessner, and S. E. Nagler, Neutron scattering in the proximate quantum spin liquid α -RuCl₃, *Science* **356**, 1055 (2017).
- [25] S. M. Winter, Y. Li, H. O. Jeschke, and R. Valentí, Challenges in design of Kitaev materials: Magnetic interactions from competing energy scales, *Phys. Rev. B* **93**, 214431 (2016).
- [26] L. Janssen, E. C. Andrade, and M. Vojta, Honeycomb-lattice Heisenberg-Kitaev model in a magnetic field: Spin canting, metamagnetism, and vortex crystals, *Phys. Rev. Lett.* **117**, 277202 (2016).
- [27] V. M. Katukuri, R. Yadav, L. Hozoi, S. Nishimoto, and J. van den Brink, The vicinity of hyper-honeycomb β -Li₂IrO₃ to a three-dimensional Kitaev spin liquid state, *Sci. Rep.* **6**, 29585 (2016).

- [28] T. Takayama, A. Kato, R. Dinnebier, J. Nuss, H. Kono, L. S. I. Veiga, G. Fabbri, D. Haskel, and H. Takagi, Hyperhoneycomb iridate β -Li₂IrO₃ as a platform for Kitaev magnetism, *Phys. Rev. Lett.* **114**, 077202 (2015).
- [29] A. A. Tsirlin and P. Gegenwart, Kitaev magnetism through the prism of lithium iridate, *Phys. Status Solidi B* **259**, 2100146 (2022).
- [30] D. Gotfryd, J. Rusnačko, K. Wohlfeld, G. Jackeli, J. Chaloupka, and A. M. Oleś, Phase diagram and spin correlations of the Kitaev-Heisenberg model: Importance of quantum effects, *Phys. Rev. B* **95**, 024426 (2017).
- [31] R. Schaffer, S. Bhattacharjee, and Y. B. Kim, Quantum phase transition in Heisenberg-Kitaev model, *Phys. Rev. B* **86**, 224417 (2012).
- [32] X.-Y. Feng, G.-M. Zhang, and T. Xiang, Topological characterization of quantum phase transitions in a spin-1/2 model, *Phys. Rev. Lett.* **98**, 087204 (2007).
- [33] L. Holleis, J. C. Prestigiacomo, Z. Fan, S. Nishimoto, M. Osofsky, G.-W. Chern, J. van den Brink, and B. Shivaram, Anomalous and anisotropic nonlinear susceptibility in the proximate Kitaev magnet α -RuCl₃, *npj Quantum Mater.* **6**, 66 (2021).
- [34] H. Kelker, History of liquid crystals, *Mol. Cryst. Liq. Cryst.* **21**, 1 (1973).
- [35] H. Kelker, Survey of the early history of liquid crystals, *Mol. Cryst. Liq. Cryst. Incorporating Nonlinear Opt.* **165**, 1 (1988).
- [36] N. D. Mermin and H. Wagner, Absence of ferromagnetism or antiferromagnetism in one- or two-dimensional isotropic Heisenberg models, *Phys. Rev. Lett.* **17**, 1133 (1966).
- [37] G. P. Alexander, Bryan Gin-ge Chen, E. A. Matsumoto, and R. D. Kamien, *Colloquium: Disclination loops, point defects, and all that in nematic liquid crystals*, *Rev. Mod. Phys.* **84**, 497 (2012).
- [38] A. Läuchli, F. Mila, and K. Penc, Quadrupolar phases of the $S = 1$ bilinear-biquadratic Heisenberg model on the triangular lattice, *Phys. Rev. Lett.* **97**, 087205 (2006).
- [39] H. Tsunetsugu and M. Arikawa, Spin nematic phase in $S = 1$ triangular antiferromagnets, *J. Phys. Soc. Jpn.* **75**, 083701 (2006).
- [40] C. Lacroix, P. Mendels, and F. Mila, *Introduction to Frustrated Magnetism: Materials, Experiments, Theory* (Springer, Berlin, 2011), Vol. 164.
- [41] M. Blume and Y. Hsieh, Biquadratic exchange and quadrupolar ordering, *J. Appl. Phys.* **40**, 1249 (1969).
- [42] W.-J. Hu, S.-S. Gong, H.-H. Lai, H. Hu, Q. Si, and A. H. Nevidomskyy, Nematic spin liquid phase in a frustrated spin-1 system on the square lattice, *Phys. Rev. B* **100**, 165142 (2019).
- [43] D. Podolsky and E. Demler, Properties and detection of spin nematic order in strongly correlated electron systems, *New J. Phys.* **7**, 59 (2005).
- [44] K. Tanaka and C. Hotta, Multiple quadrupolar or nematic phases driven by the Heisenberg interactions in a spin-1 dimer system forming a bilayer, *Phys. Rev. B* **101**, 094422 (2020).
- [45] T. Hikihara, L. Kecke, T. Momoi, and A. Furusaki, Vector chiral and multipolar orders in the spin- $\frac{1}{2}$ frustrated ferromagnetic chain in magnetic field, *Phys. Rev. B* **78**, 144404 (2008).
- [46] A. Parvej and M. Kumar, Multipolar phase in frustrated spin-1/2 and spin-1 chains, *Phys. Rev. B* **96**, 054413 (2017).
- [47] J. Sudan, A. Läuscher, and A. M. Läuchli, Emergent multipolar spin correlations in a fluctuating spiral: The frustrated ferromagnetic spin- $\frac{1}{2}$ Heisenberg chain in a magnetic field, *Phys. Rev. B* **80**, 140402(R) (2009).
- [48] J. Nasu, Y. Kato, J. Yoshitake, Y. Kamiya, and Y. Motome, Spin-liquid-to-spin-liquid transition in Kitaev magnets driven by fractionalization, *Phys. Rev. Lett.* **118**, 137203 (2017).
- [49] M. O. Takahashi, M. G. Yamada, D. Takikawa, T. Mizushima, and S. Fujimoto, Topological nematic phase transition in Kitaev magnets under applied magnetic fields, *Phys. Rev. Res.* **3**, 023189 (2021).
- [50] K. Penc and A. M. Läuchli, Spin nematic phases in quantum spin systems, in *Introduction to Frustrated Magnetism: Materials, Experiments, Theory*, edited by C. Lacroix, P. Mendels, and F. Mila (Springer, Berlin, 2011), pp. 331–362.
- [51] H.-J. Grafe, S. Nishimoto, M. Iakovleva, E. Vavilova, L. Spillecke, A. Alfonsov, M.-I. Sturza, S. Wurmehl, H. Nohji, H. Rosner *et al.*, Signatures of a magnetic field-induced unconventional nematic liquid in the frustrated and anisotropic spin-chain cuprate LiCuSbO₄, *Sci. Rep.* **7**, 6720 (2017).
- [52] C. E. Agrapidis, J. van den Brink, and S. Nishimoto, Ground state and low-energy excitations of the Kitaev-Heisenberg two-leg ladder, *Phys. Rev. B* **99**, 224418 (2019).
- [53] A. Catuneanu, E. S. Sørensen, and H.-Y. Kee, Nonlocal string order parameter in the $S = \frac{1}{2}$ Kitaev-Heisenberg ladder, *Phys. Rev. B* **99**, 195112 (2019).
- [54] S. R. White, Density matrix formulation for quantum renormalization groups, *Phys. Rev. Lett.* **69**, 2863 (1992).
- [55] S. R. White, Density-matrix algorithms for quantum renormalization groups, *Phys. Rev. B* **48**, 10345 (1993).
- [56] M. Kumar, Z. G. Soos, D. Sen, and S. Ramasesha, Modified density matrix renormalization group algorithm for the zigzag spin- $\frac{1}{2}$ chain with frustrated antiferromagnetic exchange: Comparison with field theory at large J_2/J_1 , *Phys. Rev. B* **81**, 104406 (2010).
- [57] See Supplemental Material at <http://link.aps.org/supplemental/10.1103/PhysRevB.109.L220403> for the following topics in relation to the main text: (I) Schematic picture of quadrupolar ordered states, (II) wave-function analysis in two-leg ladder, (III) quadrupolar order and correlation in two-leg ladder from ED, (IV) finite-size effects in the quadrupolar correlation functions in two-leg ladder, and (V) quadrupolar phases in 2D honeycomb lattice, which includes Refs. [54–56].
- [58] N. Shannon, T. Momoi, and P. Sindzingre, Nematic order in square lattice frustrated ferromagnets, *Phys. Rev. Lett.* **96**, 027213 (2006).
- [59] R. Yadav, N. A. Bogdanov, V. M. Katukuri, S. Nishimoto, J. Van Den Brink, and L. Hozoi, Kitaev exchange and field-induced quantum spin-liquid states in honeycomb α -RuCl₃, *Sci. Rep.* **6**, 37925 (2016).